Newer Modalities for Imaging Nonischemic Cardiomyopathy

Shuchita Gupta, MD,[1] Aman M. Amanullah MD, PhD, FACC[2,3]
[1]Thomas Jefferson University Hospital, Philadelphia, PA; [2]Einstein Institute for Heart and Vascular Health, Einstein Medical Center, Philadelphia, PA; [3]Sidney Kimmel Medical College at Thomas Jefferson University, Philadelphia, PA

Cardiomyopathies are practically classified as either ischemic or nonischemic based on the presence or absence of coronary artery disease. Although conventional two-dimensional echocardiography can assess left ventricular ejection fraction, wall motion, and diastolic function, it does not fully capture myocardial mechanics or tissue characterization, and does not accurately identify patients with nonischemic cardiomyopathy (NICMP) at risk for sudden cardiac death. This article discusses advanced imaging modalities for assessment of NICMP, namely, three-dimensional echocardiography, strain imaging, cardiac magnetic resonance, cardiac computed tomography, and sympathetic innervation imaging.

[Rev Cardiovasc Med. *2015;16(1):51-67 doi: 10.3909/ricm0748]*

KEY WORDS

Nonischemic cardiomyopathy • Three-dimensional echocardiography • Myocardial deformation • Cardiac magnetic resonance • Cardiac computed tomography • Sympathetic innervation imaging

A practical method of classifying cardiomyopathies on imaging has been to separate them into ischemic and nonischemic categories based on the presence or absence of obstructive coronary artery disease on angiography or on wall motion abnormalities on two-dimensional echocardiography. Echocardiography can quantify the severity of left ventricular (LV) systolic and diastolic dysfunction; in most cases, however, it does not identify the etiology of nonischemic cardiomyopathy (NICMP), as tissue characterization is not possible with routine echocardiography.

Although LV ejection fraction (LVEF) is universally used as an indicator of systolic dysfunction of the left and right ventricles, it is too simplistic to capture the entire gamut of myocardial abnormalities that accompany myocardial dysfunction. Moreover, it correlates most closely with radial performance of the myocardium while ignoring the contribution of longitudinal contraction and deformation. Systolic

mechanics, however, occur in the circumferential, radial, and longitudinal directions, and more than one modality is needed to capture myocardial motion in all directions. Moreover, reduced LVEF is a nonspecific indicator of fatal ventricular arrhythmias and may not be the best indicator of the need for defibrillator placement when used alone.[1]

This article discusses various advanced imaging modalities to assess myocardial function in NICMP, including newer echocardiographic modalities, cardiac magnetic resonance imaging (CMR), and sympathetic innervation imaging.

Three-dimensional Echocardiography

Recent development of transesophageal and transthoracic multiplane ultrasound probes has enabled the acquisition of rotational images at defined interval angles around a fixed axis, leading to the development of three-dimensional (3D) echocardiography.[2] Images are collected over a 180° rotation at set intervals. Sequential images are gated to both electrocardiography (ECG) and respiration to avoid reconstruction artifacts. Approximately four to six serial images are sufficient for volume reconstructions of the left ventricle, whereas more images are needed to visualize rapidly moving structures, such as mitral and aortic valves. Once the two-dimensional (2D) images have been obtained, they are processed offline with customized or commercially available software.[3]

To circumvent the issues associated with offline processing, real-time 3D echocardiography was developed. This technique uses matrix array transducers with more than 3000 imaging elements in a transducer.[4] The ability to extract hemodynamic information from 3D color Doppler ultrasonography is also being researched.

At present, 3D echocardiography serves to complement the traditional 2D echocardiographic examination. Application of newer endocardial border detection techniques permits accurate assessment of LV volume, mass, and EF with 3D echocardiography (Figure 1), which is particularly useful in the appropriate selection of patients for implantable cardioverter defibrillator (ICD) placement and cardiac resynchronization therapy (CRT).[5] Assessment of the right ventricle is severely limited by 2D echocardiography, as its asymmetric pyramidal shape does not conform to any geometric assumptions. Thus, 3D echocardiography is particularly valuable to assess the right ventricular (RV) chamber shape, volumes, and RVEF in patients with NICMP, especially in those with predominant involvement of the right ventricle, such as those with arrhythmogenic RV dysplasia (ARVD).[6]

Recent development of transesophageal and transthoracic multiplane ultrasound probes has enabled the acquisition of rotational images at defined interval angles around a fixed axis, leading to the development of three-dimensional echocardiography.

Patients with dilated cardiomyopathy (DCM) frequently develop functional mitral regurgitation (FMR) due to annular dilatation, mitral valve tenting, and tethering of the mitral leaflets. The 3D echocardiography technique has identified changes in annular shape

Figure 1. Measuring left ventricular ejection fraction using three-dimensional echocardiography. The three-dimensional full volume image is cropped and rotated along multiple planes to isolate the left ventricle. Automated border detection algorithm is applied and a cast of the endocardium is created. The cast is automatically divided into wall segments. Regional and segmental volume changes are tracked over the cardiac cycle for regional wall motion and dyssynchrony analyses.

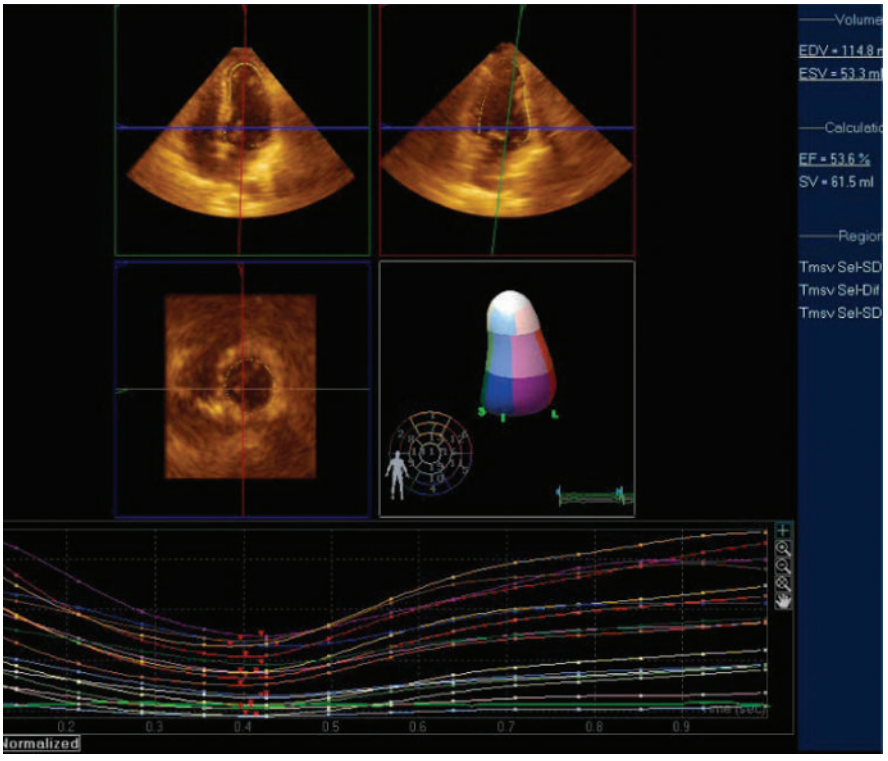

occurring with FMR, thus contributing to our understanding of the pathophysiology of FMR.[7,8] Using 3D echocardiography, the mitral annulus size and mitral valve tenting volume can be assessed. Using 3D color Doppler, accurate quantification of FMR can be done by calculating effective regurgitant orifice area and regurgitant volume, which correlate well with CMR-derived parameters.[9]

Patients with heart failure also develop pulmonary hypertension and functional tricuspid regurgitation, which is associated with increased morbidity and mortality. Real-time 3D echocardiography of the tricuspid valve has provided insight into the mechanism of tricuspid regurgitation. The normal tricuspid annulus has a bimodal shape with distinct high and low points. With functional tricuspid regurgitation, the annulus becomes larger, more planar, and circular.[10]

Another application of 3D echocardiography is in dyssynchrony evaluation. Real-time 3D echocardiography allows for a comparison of synchrony between segments of the left ventricle in the same cardiac cycle. Kapetanakis and colleagues[11] calculated a systolic dyssynchrony index from the dispersion of time to minimum regional volume for all 16 LV segments and found this to predict reverse remodeling after CRT. However, lower spatial and temporal resolution is a limiting factor.

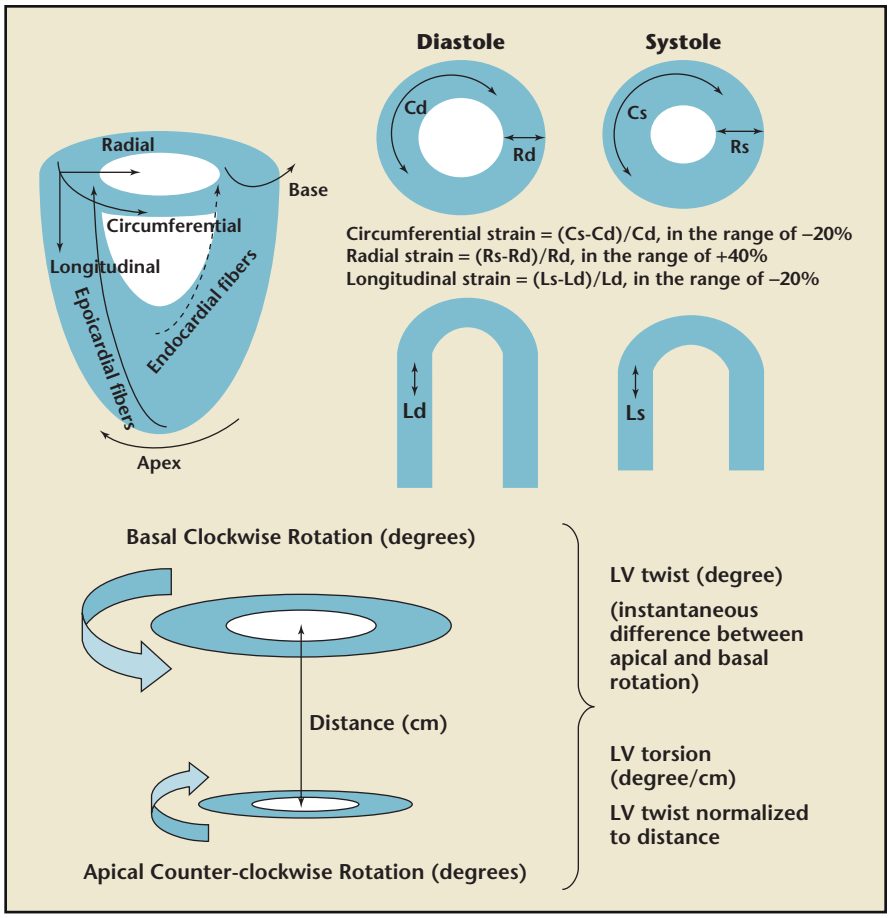

Figure 2. Components of myocardial deformation. *Straight arrows* show the direction of strain measurement. *Curved arrows* indicate the direction of motion. Cd, circumferential diastolic strain; Cs, circumferential systolic strain; Ld, longitudinal diastolic strain; Ls, longitudinal systolic strain; LV, left ventricular; Rd, radial diastolic strain; Rs, radial systolic strain.

Myocardial Deformation

Strain describes myocardial deformation—the fractional change in length of a myocardial segment (unitless, usually expressed as a percentage)—whereas strain rate is the rate of change in strain (1/s). Displacement reflects the distance that a certain feature, such as a speckle or cardiac structure, has moved between two consecutive frames, whereas velocity reflects displacement per unit of time—how fast the location of a feature changes (cm/s). Displacement and velocity are vectors and have a direction.[12]

In the LV myocardium, the myofiber geometry changes from a right-handed helix in the subendocardium to a left-handed helix in the subepicardium.[13] The overall direction of rotation is counterclockwise at the apex and clockwise at the base. LV twist is defined as the difference between apical and basal rotation, whereas LV torsion is the twist normalized to distance (Figure 2).

Tissue Doppler (TD)-derived strain and strain rate were the first methods used to quantify myocardial deformation (Figure 3), but angle dependence and noise interference make this method less desirable. Speckle-tracking echocardiography (STE) is an angle-independent method for strain analysis. Speckles are small, temporally stable myocardial features formed due to constructive and destructive interference of ultrasound backscattered from structures smaller than the ultrasound wavelength. Using these speckle patterns (speckle tracking) to identify specific points in

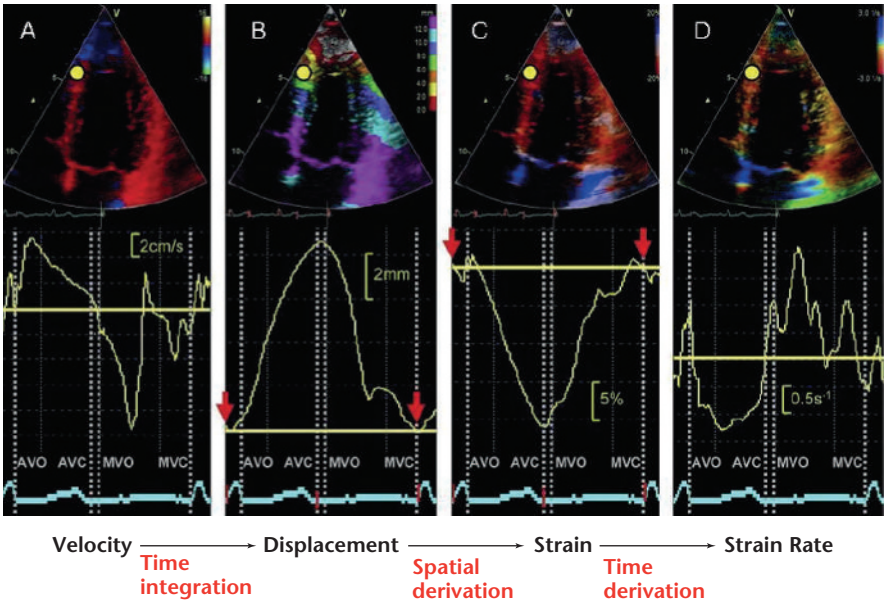

Figure 3. Parameters of myocardial deformation derived from one region of interest *(yellow dot)* using tissue Doppler imaging. **(A)** Velocity. **(B)** Displacement. **(C)** Strain. **(D)** Strain rate.

the myocardium, strain can be recorded. STE can analyze longitudinal and radial deformation of all LV segments from apical views, and radial strain and circumferential strain (CS) of all LV segments from the short-axis views (Figure 4).[14]

Velocity-Vector Imaging

Velocity-vector imaging (VVI) is an advanced echocardiographic method derived from STE. With a pattern-matching algorithm, VVI can accurately track speckles frame by frame, and, through reconstruction of the deformation and motion, the motion of flow and tissue can be analyzed. The advantage of VVI is that it is self-updating. Special reference settings are applied, including valvular annulus, chamber borders, and tissue motion, as well as the relatively static reference point provided by the software. All these features provide precision to the tracking process. VVI is faster than conventional STE, and obtaining each patient's parameters takes approximately 5 minutes, which is faster than a routine STE study. The segmental EF contribution of each segment may be obtained with VVI.[15] Time to peak velocity, time to peak strain, and strain rate can be calculated.[16] Using VVI, patients with DCM were found to have reduced LV peak twist and torsion, with a significant correlation between EF and LV twist.[17]

Using VVI, patients with DCM were found to have reduced LV peak twist and torsion, with a significant correlation between EF and LV twist.

3D STE

An advance in strain imaging is the use of 3D STE. With 2D STE, speckles may not stay in the imaging plane at all times, whereas 3D STE can track motion of speckles irrespective of their direction, as long as they remain within the selected scan volume. 3D STE is applied to full-volume 3D echocardiographic images.

Applications of Strain Imaging

Longitudinal LV mechanics is affected predominantly by the subendocardial region, and is most vulnerable to myocardial disease. In the initial stages of cardiomyopathy, midmyocardial and epicardial functions are unaffected; therefore, CS is normal. With acute transmural insult or disease progression, midmyocardial and epicardial dysfunction occurs with concurrent reduction in LV circumferential mechanics. Strain patterns in healthy individuals and in disease states are summarized in Table 1.

Brown and colleagues[18] explored whether global longitudinal strain (GLS) could be an alternative to the measurement of LVEF, using MRI-derived EF (MRI-EF) as the reference standard in 62 patients. They also compared GLS with 3D echocardiography-derived EF (3D-EF). The correlation of GLS with MRI-EF ($r = -0.69$; $P < .0001$) was comparable to that between 3D-EF and MRI ($r = 0.80$; $P < .0001$). In those with > 6 abnormal segments, the correlation of GLS with MRI-EF improved significantly ($r = -0.77$; $P < .0001$) and was similar to 3D-EF ($r = 0.76$; $P < .0001$). Stanton and colleagues[19] studied the prognostic value of GLS beyond conventional parameters in 546 patients. GLS provided incremental value in subgroups with EF $>$ 35% and those with and without wall motion abnormalities. A GLS $\geq -12\%$ was found to be equivalent to an EF $\leq$ 35% for the prediction of prognosis.

In the Penn Heart Failure Study, the prognostic utility of strain and strain rate were evaluated in 416 patients with chronic systolic heart failure (76% with NICMP). Reduced strain and strain rate correlated strongly with higher New York Heart Association (NYHA) class, greater N-terminal prohormone

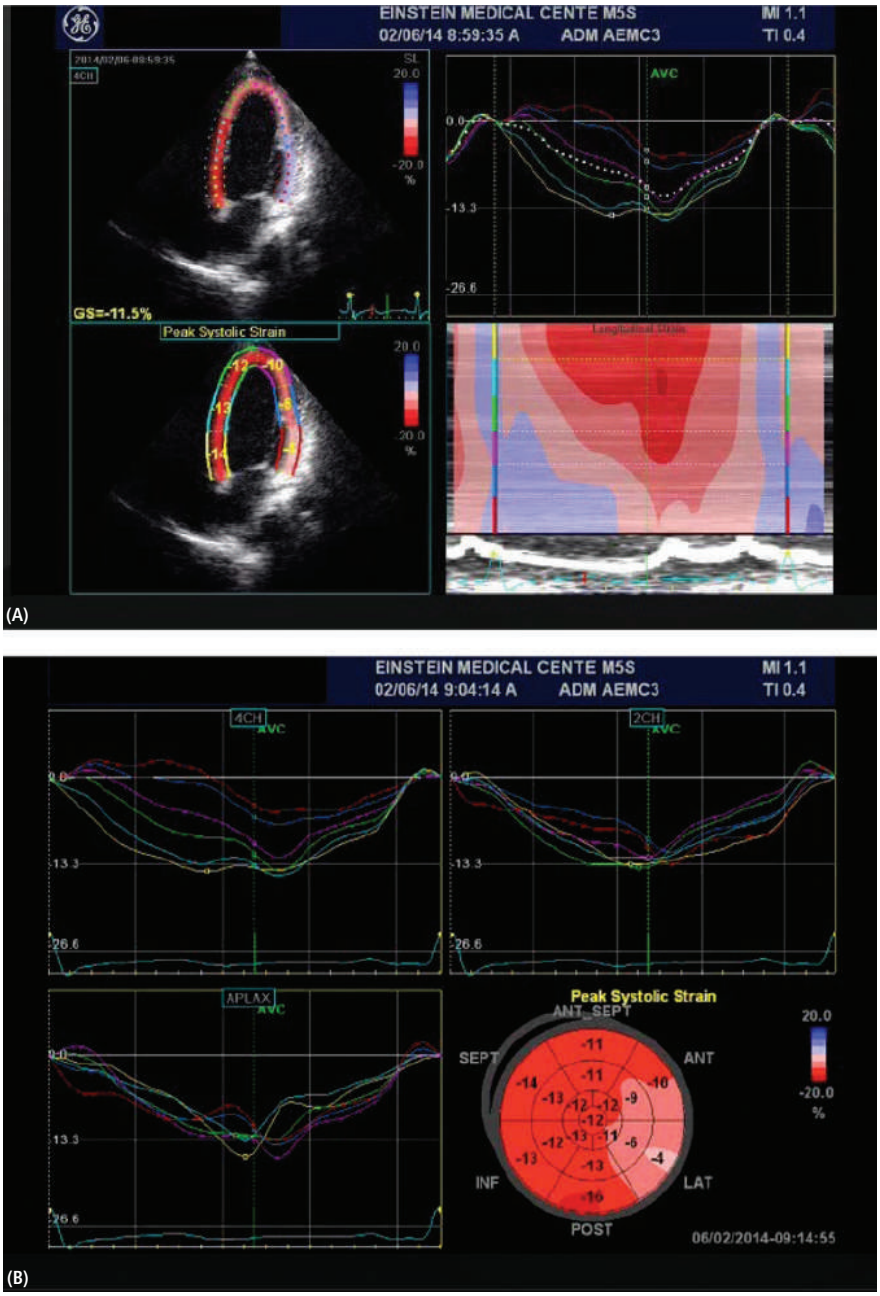

Figure 4. Speckle-tracking echocardiography-derived longitudinal strain in a patient with cardiomyopathy with a left ventricular ejection fraction of 40%. **(A, *top left*)** Peak longitudinal strain in aapical four-chamber view. **(A, *top right*)** Wave form display. **(A, *bottom left*)** Quantitative parametric overlay. **(A, *bottom right*)** Color M-mode display. **(B)** Bull's eye presentation of strain.

brain natriuretic peptide levels, and increased chamber size. Strain in all three dimensions (longitudinal, circumferential, and radial) and strain rate in two dimensions (longitudinal and circumferential) were independently associated with an increased risk of adverse cardiovascular outcomes in multivariable models adjusted for clinical variables. Addition of strain, but not strain rate to EF, led to a significantly improved prediction at 1 year (area under the curve [AUC] 0.697 vs 0.633; $P = .032$) and 5 years (AUC 0.700 vs 0.638; $P = .001$).[20] This study suggests that strain could be used to identify high-risk patients and aid in the selection of heart failure patients for advanced therapies.

STE is particularly useful for identification of systolic dysfunction in patients with normal EF as measured by conventional echocardiography. In a study of patients with hypertensive heart disease and heart failure with preserved LVEF (HFpEF), those with hypertensive heart disease had lower longitudinal strain (LS), but increased CS, whereas patients with HFpEF had markedly reduced LS and CS values.[21] Patients with hypertrophic cardiomyopathy (HCM) have reduced LS and increased CS; the former correlates with symptoms.[22] Left atrial LS was studied as a marker of increased LV pressure, and found to be reduced in patients with HCM.[23] Patients with cardiac amyloidosis have decreased LS at the base with relative apical sparing, which helps distinguish this condition from other causes of LV hypertrophy.[24] Reduced LS has been demonstrated to predict reduced survival in patients with light-chain amyloidosis.[25]

Decreased LS can be used to assess cardiotoxicity of chemotherapeutic drugs such as anthracyclines (doxorubicin, epirubicin) and trastuzumab before a drop in LVEF is seen.[26] In a recent systematic review, 13 peer-reviewed publications that assessed echocardiography-based myocardial deformation parameters in a total of 384 patients treated with anthracycline-inclusive chemotherapeutic regimens were studied. Most of these were single-center cohort studies involving patients with breast and hematologic malignancies. Earlier studies used TD imaging–based strain, whereas

STE is particularly useful for identification of systolic dysfunction in patients with normal EF as measured by conventional echocardiography.

more recent contemporary studies predominantly used 2D STE. Despite variability in data regarding patient demographics, cancer type, strain techniques, and follow-up, a uniform finding was that changes in myocardial deformation occurred earlier than changes in LVEF and at anthracycline doses lower than what were historically thought to be cardiotoxic. A 10% to 15% early reduction in GLS by STE during therapy appeared to be useful to predict cardiotoxicity.[27] Reductions in strain rate have been detected with cumulative doses of anthracycline (epirubicin) as low as 200 mg/m^2, and these changes correspond to increases in levels of reactive oxygen species, the purported mechanism of anthracycline-induced cardiotoxicity.[28] In a study of anthracycline-treated survivors of childhood cancer, 3D STE revealed impaired strain values in treated patients compared with control subjects, and the extent of derangement correlated with cumulative anthracycline dose.[29] In studies involving patients receiving trastuzumab, GLS was again found to be the best predictor of future decline in LVEF.[30,31] These studies suggest that strain imaging can be useful for early detection of chemotherapy-induced cardiotoxicity so that treatment with reverse remodeling agents can be initiated. According to an expert consensus for multimodality imaging evaluation of adult patients during and after cancer therapy, published by the American Society of Echocardiography (ASE), either a drop in GLS of $>$ 15% from baseline after starting anthracycline/trastuzumab therapy without a drop in LVEF or a GLS value at any time below the lower limit of normal should be considered evidence of subclinical LV dysfunction. The ASE also recommends using the same vendor-specific ultrasound machine for strain measurements for longitudinal follow-up of cancer patients.[32]

RV LS has also been analyzed in patients with cardiomyopathy. In a study of 171 patients with LVEF < 35%, the degree of impairment in RV strain was associated with increasing NYHA class, greater LV end-diastolic volumes, reduced LVEF, worse LV diastolic dysfunction, and worse RV systolic and diastolic dysfunction. RV strain $\geq -14.8\%$ predicted adverse events after adjustment for age, LVEF, and indices of elevated left and right atrial pressures.[33] RV LS assessed by STE in patients with end-stage cardiomyopathy has been used to predict the risk of RV failure following implantation of an LV assist device (LVAD).[34] In a study of 117 patients undergoing LVAD implantation, RV free-wall peak strain assessed using VVI was significantly lower in patients who developed RV failure after implantation versus those who did not (-9.0% vs -12.2%; $P < .01$).[35]

Strain imaging has been used in the assessment of significant LV dyssynchrony to predict response to CRT in patients with NICMP. Septal-lateral LV dyssynchrony can be assessed by calculating delay

TABLE 1

Strain Pattern in Healthy Subjects and in Those With Pathologic Conditions

Parameter	Healthy	Dilated Cardiomyopathy	Hypertrophic Cardiomyopathy	Heart Failure With Preserved Ejection Fraction
Circumferential strain (%)	− 15 to −20	Decreased magnitude	Decreased magnitude (mainly in the septum and fibrotic tissue)	Decreased magnitude
Longitudinal strain (%)	− 15 to −20	Decreased magnitude	Decreased magnitude	Decreased magnitude
Radial strain (%)	30 to 40	Decreased		
Rotation base (degrees)	− 4 to −7 (clockwise)	—		
Rotation apex (degrees)	5 to 10 (counterclockwise)	—		Increased
Twist (degrees)	~ 15	Shortened and reduced ~ 50%	Increased	Initially increased, further normalization

Adapted from Castillo E et al.[61]

in TD-derived LS values between septal and lateral walls.[36] Radial strain calculated from TD velocity data from the anteroseptum and posterior wall in the mid LV short-axis view has been used to identify radial dyssynchrony.[37] STE applied to midventricular short-axis images determines radial strain from multiple points averaged to six standard segments.[38] VVI has also been used with dyssynchrony defined by the greatest opposing wall peak longitudinal systolic velocity delay.[39]

The role of dyssynchrony evaluation has come into question since the publication of the Predictors of Response to CRT (PROSPECT) study,[40] which was an observational study of CRT response (defined by an improved clinical score and $\geq$ 15% reduction in LV end-systolic volume at 6 mo) in 426 patients requiring CRT. Echocardiographic parameters of dyssynchrony in this study had low sensitivity and reliability for predicting response to CRT. However, this study included only M-mode and TD imaging for dyssynchrony analysis, and there was wide interobserver variability in M-mode and TD imaging measurements.[41] Thus, this cannot be regarded as a definitive study, and further randomized trials using STE and 3D echocardiography-derived strain are needed to define the utility of echocardiographic dyssynchrony evaluation in selecting patients for CRT.

Strain imaging has been used in the assessment of significant LV dyssynchrony to predict response to CRT in patients with NICMP. Septal-lateral LV dyssynchrony can be assessed by calculating delay in TD-derived LS values between septal and lateral walls.

CMR

In recent years, CMR has emerged as a useful imaging modality for patients with cardiomyopathies. Cine CMR is used in the assessment of cardiac function and morphology by reconstructing ECG-gated images. It provides accurate assessment of LV and RV mass and volume, EF, and global and regional segmental wall motion. Morphologic characteristics associated with specific cardiomyopathies, such as fatty infiltration and RV aneurysms in ARVD, and septal and apical hypertrophy with or without LV outflow tract obstruction in HCM, can be easily detected with cine CMR (Figure 5). CMR is considered the gold standard for assessment of RV volumes and EF.

CMR is valuable in the identification of LV noncompaction cardiomyopathy. This is a rare form of NICMP, which is believed to be caused by an arrest of the normal process of compaction of a spongy meshwork of fibers in the ventricle from the epicardium to endocardium and from the base to the apex between 5 and 8 weeks of embryonic development.[42] Multiple prominent trabeculations and intertrabecular recesses are seen on imaging. A

Figure 5. Cardiac magnetic resonance imaging in arrhythmogenic right ventricular dysplasia. Double inversion recovery sequences without and with fat suppression; fatty infiltration of right ventricular wall.

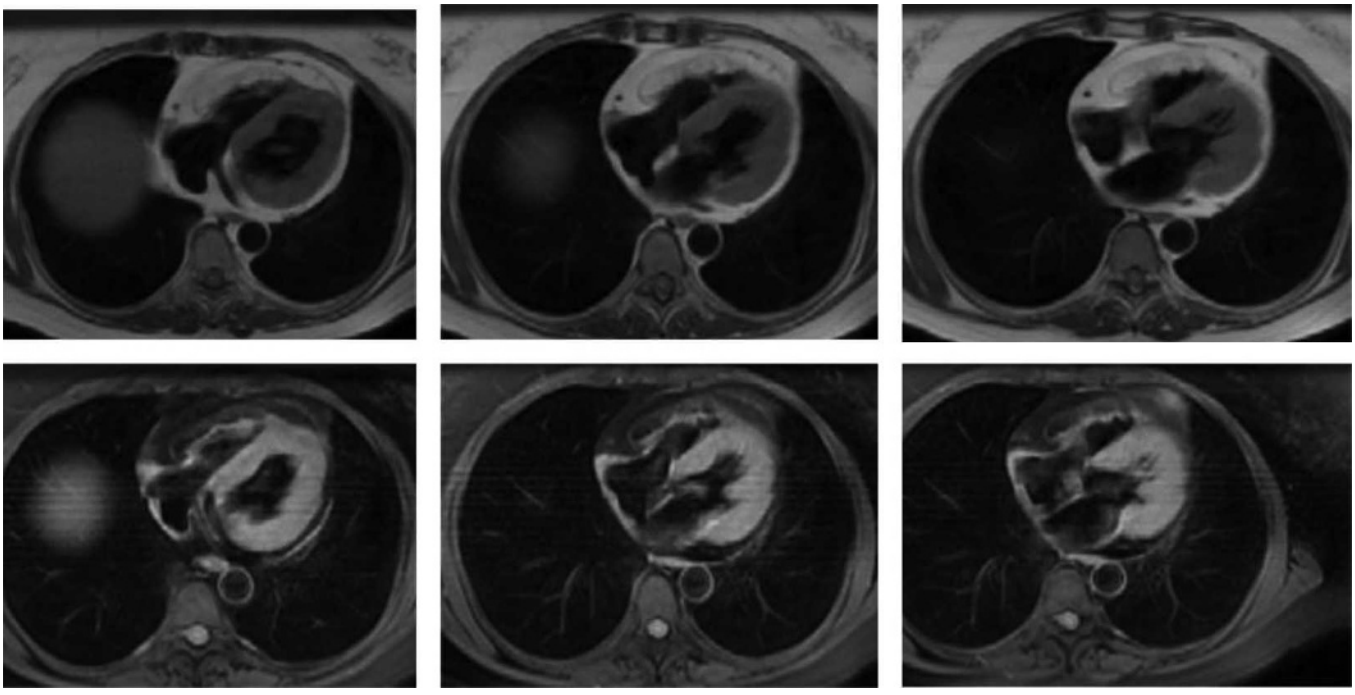

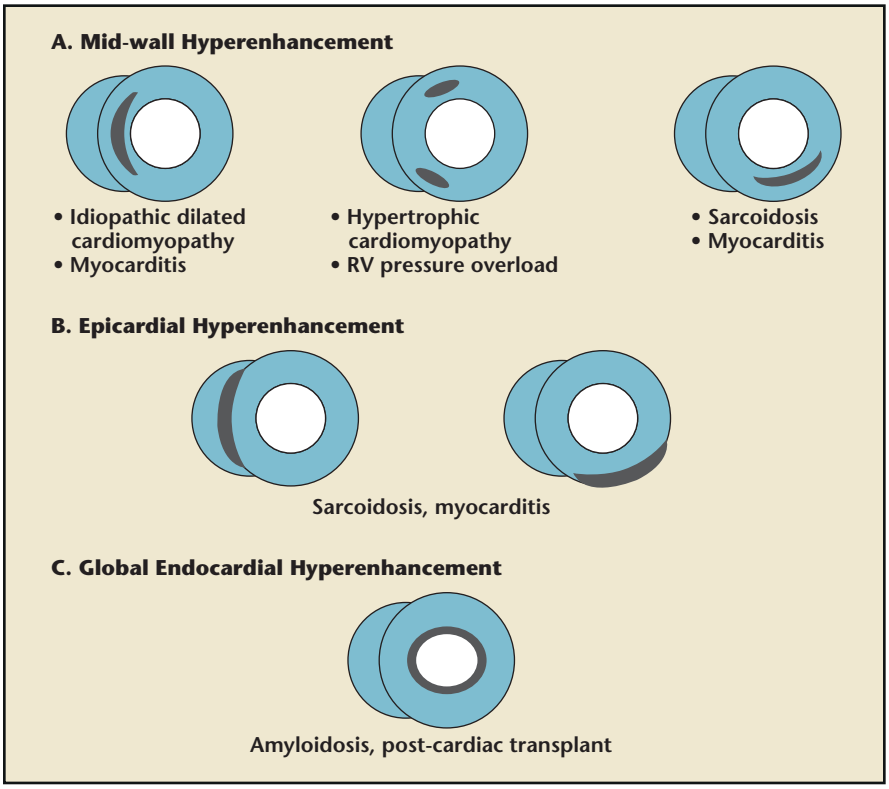

Figure 6. Patterns of hyperenhancement on delayed-enhancement cardiac magnetic resonance imaging in common nonischemic cardiomyopathies.

ratio of 2:3 between noncompacted and compacted myocardium at end-diastole with CMR is considered diagnostic.[43]

Although cine CMR is useful for functional assessment, delayed-enhancement CMR (DE-CMR) helps in tissue characterization, particularly in assessment of myocardial fibrosis. In fact, the unique ability of DE-CMR to provide a noninvasive histologic assessment, thus assisting in identification of specific etiologies of cardiomyopathy without the need for endomyocardial biopsy, represents its most attractive clinical potential.

… the unique ability of DE-CMR to provide a noninvasive histologic assessment, thus assisting in identification of specific etiologies of cardiomyopathy without the need for endomyocardial biopsy, represents its most attractive clinical potential.

Gadolinium chelates used for DE-CMR are extracellular contrast agents that cannot cross myocyte cell membranes. Moreover, normal myocardium has densely packed myocytes and very little extracellular space for gadolinium chelates to accumulate. Hyperenhancement seen in acute myocardial infarction is due to rupture of myocyte cell membranes and increased entry of gadolinium into cells, whereas that in fibrosis is due to expansion of the interstitial space from collagenous scar formation.

First-pass imaging is performed 5 minutes after administration of gadolinium chelates, whereas delayed imaging is performed within 20 minutes after injection. Late gadolinium enhancement (LGE) on DE-CMR in a coronary territory indicates prior myocardial infarction. In NICMP, there may be no LGE or it may be present in a noncoronary distribution. Various patterns of LGE in NICMP are shown in Figure 6, and CMR findings in common causes of NICMP are summarized in Table 2. Delayed enhancement in a subepicardial distribution is unusual, but highly suggestive of myocarditis.

In a study of 472 patients with idiopathic DCM referred for CMR imaging, midwall hyperenhancement was seen in 142 patients. After adjustment for LVEF and other conventional prognostic factors, both the presence and the extent of midwall fibrosis were independently and incrementally associated with all-cause mortality, cardiovascular mortality, cardiac transplantation, and sudden cardiac death (SCD).[44] In another study of patients with DCM, midwall hyperenhancement was an independent predictor of morbidity and mortality in patients undergoing CRT.[45] More recently, in a pooled analysis of 9 studies comprising 1488 patients and a mean follow-up of 30 months, 38% had LGE. These patients had increased overall mortality, heart failure hospitalization, and SCD/aborted SCD compared with those without LGE.[46] In another study of 228 patients with NICMP without heart failure, those with LGE had a greater risk of developing heart failure and aborted SCD.[47] The presence and extent of LGE was also shown to be associated with increased levels of transcardiac troponin T in patients with NICMP with heart failure, indicating that ongoing cardiac damage correlates with degree of myocardial fibrosis.[48] In patients with cardiac sarcoidosis, LGE was associated with increased risk of both atrial and ventricular arrhythmias.[49] These studies suggest that evidence of

TABLE 2

Cardiac Magnetic Resonance Features of Various Nonischemic Cardiomyopathies

Type	Cine CMR	LGE Pattern
Idiopathic dilated cardiomyopathy	Systolic dysfunction of left ventricle ± right ventricle LV dilatation Thrombus Valvular lesions	Absent or midwall fibrosis Epicardial fibrosis Noncoronary distribution
Myocarditis	Systolic dysfunction of LV T2-weighted imaging for myocardial edema shows extent of acute inflammation Steady-state free precession technique for imaging edema	Subepicardial (with active myocarditis) or midwall fibrosis, rarely subendocardial, lateral wall involvement frequent Eosinophilic myocarditis: subendocardial LGE may be seen
Hypertrophic cardiomyopathy	Abnormal LV hypertrophy (asymmetrical septal, apical, localized, or concentric) Systolic anterior motion of the anterior mitral leaflet, mitral regurgitation Dynamic outflow tract obstruction, apical aneurysms, myocardial clefts, and papillary muscle abnormalities	Patchy, multifocal, predominantly mid-wall More common in hypertrophied areas and the interventricular septum RV insertion sites of the septum
Amyloidosis	Homogenously thickened myocardium, Thickened interatrial septum and valve leaflets Pleural and pericardial effusions	Widespread subendocardial hyperenhancement often including the interatrial septum and right ventricle
Sarcoidosis	Localized areas of wall thinning Regional wall motion abnormalities with high signal intensity on T2-weighted images	Patchy, midwall, subepicardial, or even subendocardial Predilection to involve the basal and midseptal segments RV free wall may be involved
Iron overload	Findings of dilated cardiomyopathy with reduced myocardial T2 values	Unknown
ARVD	Focal thinning Segmental aneurysms Regional and global RV dilation Depressed function	RV and/or LV LGE indicates intramyocardial fibrofatty replacement
LV noncompaction	Extensive trabeculations Intratrabecular recesses, Absence of well-formed papillary muscles	Various patterns

ARVD, arrhythmogenic right ventricular dysplasia; CMR, cardiac magnetic resonance; LGE, late gadolinium enhancement; LV, left ventricular; RV, right ventricular.

fibrosis is a poor prognostic marker in patients with NICMP and may assist in selection of patients at high risk of SCD for ICD implantation.

DE-CMR detects fibrosis on the basis of the difference in signal intensity between an enhanced area and the normal myocardium. Thus, it detects localized fibrosis reliably, but not diffuse fibrosis. T1-mapping techniques allow assessment of diffuse fibrosis by direct quantification of myocardial T1 time.[50,51] In the setting of an increase in collagen fibers (and thus extracellular space), T1 time decreases after contrast administration.[52] Direct measurement of extracellular volume has also been developed for detection and quantification of diffuse myocardial fibrosis. Myocardial extracellular volume is measured as the percent of tissue comprised of extracellular space and has been shown to correlate with collagen volume fraction.[53]

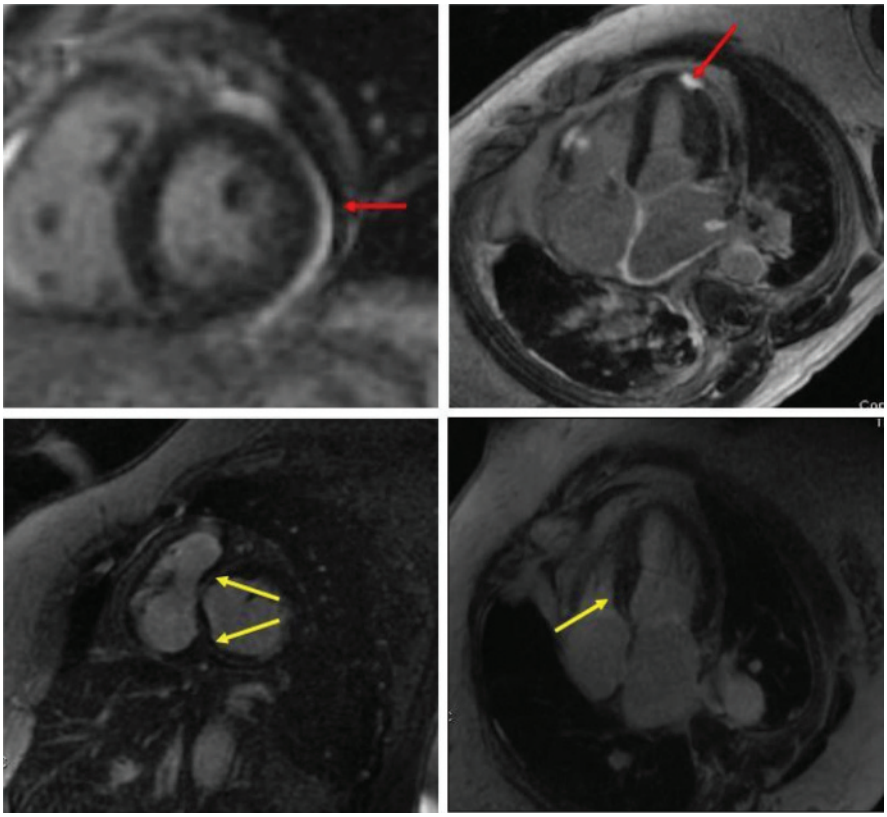

Figure 7. Cardiac magnetic resonance imaging of sarcoidosis showing patchy foci of subepicardial delayed hyperenhancement (*red arrows*) and basal septal midmyocardial hyperenhancement (*yellow arrows*).

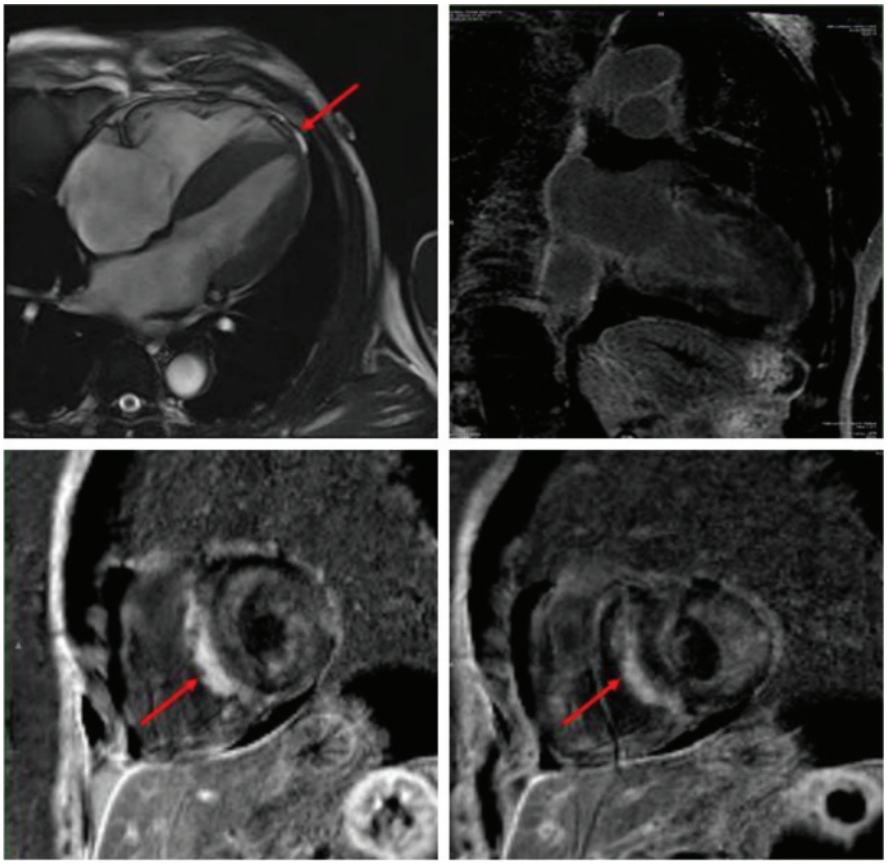

Figure 8. Cardiac magnetic resonance imaging in amyloidosis showing left ventricular hypertrophy and patchy, confluent nonterritorial areas of delayed hyperenhancement throughout the left ventricle in subendocardial, midmyocardial, and subepicardial distribution (*red arrows*).

CMR is valuable in the diagnosis of cardiac sarcoidosis (Figure 7). It can detect both the active inflammatory phase as well as the chronic phase of fibrosis and scarring of cardiac sarcoidosis. The inflammatory phase is characterized by focal wall thickening due to infiltration or edema, combined with wall motion abnormalities seen on T1-weighted (cine) images, increased signal intensity on T2-weighted images, and early gadolinium enhancement.[54] Wall thinning and LGE representing scarring and fibrosis are more common in the chronic phase.[55] The basal septum, basal and lateral segments of the LV, and the papillary muscles are frequently involved. Widespread LGE may correlate with absence of LV functional improvement and a high incidence of adverse outcomes in patients with cardiac sarcoidosis after steroid therapy.[56] In a study of patients with systemic sarcoidosis, the presence of LGE was the best independent predictor of potentially lethal events, as well as aborted SCD, or appropriate defibrillator discharges.[57] Thus, the presence of LGE in patients with cardiac sarcoidosis may help risk stratify them for ICD placement.

LGE CMR has proved to be useful in diagnosis of cardiac amyloidosis (Figure 8). An early CMR study in cardiac amyloidosis described altered gadolinium kinetics and a global subendocardial pattern of LGE.[58] Subsequently, studies using CMR to distinguish between patterns of cardiac amyloidosis in light chain (AL) amyloidosis and hereditary transthyretin-associated (ATTR) amyloidosis have been published. In one study comparing both types of cardiac amyloidosis, cardiac ATTR amyloidosis was associated with significantly higher LV mass index, higher LV volumes, and lower LVEF compared with

cardiac AL amyloidosis. Pleural and pericardial effusions were more common in cardiac AL amyloidosis. In cardiac ATTR amyloidosis, LGE was more extensive, with a higher prevalence of transmural LV LGE as well as of RV LGE.[59] In patients with ATTR amyloidosis, preclinical cardiac amyloidosis has been detected even with isolated neurologic involvement and normal LV wall thickening. In a study of 53 patients with ATTR, diffuse LGE was seen only in those with clinical manifestations of cardiac amyloidosis, whereas those with subclinical cardiac amyloidosis had mostly focal LGE.[60] These studies indicate that noninvasive diagnosis of type of cardiac amyloidosis is possible, which is clinically relevant given the efficacy of chemotherapy for AL amyloidosis.

Deformation analysis can be carried out using two MRI techniques. MR myocardial tagging superimposes black lines or grids on the myocardium. The deformation of tracked tags in all directions throughout the cardiac cycle allows quantification of several objective (ie, operator-independent) components of motion and is comparable with STE.[61] Tissue phase mapping directly encodes the velocity of myocardial motion into the MRI signal and offers high spatial resolution of the functional information (1-3 mm).[62] Being dependent on breath-held measurements, both these methods have limited temporal resolution.

Aside from strain assessment in all three directions, LV rotation and torsion assessment is also possible with these techniques. In a study of LV torsion by myocardial tagging, impaired systolic torsion was seen in DCM with reversal of apical rotation at mid-systole. The amplitude of peak torsion was correlated with LVEF ($r = 0.74$; $P < .001$).[63] Patients with HCM have relatively preserved net LV twist, although the apex-to-base progression of LV twist sequence is altered.[64] Rotation at the mid-LV level becomes clockwise, similar to the direction of rotation of the LV base (opposite of normal). There is regional heterogeneity of LV twist, reducing the gradient of LV rotation for the basal aspect of the LV, while exaggerating it toward the LV apex.[65] Alcohol septal ablation transiently decreases LV twist, but twist returns to higher than baseline values afterward.[66]

As most cardiomyopathies initially lead to subendocardial dysfunction, LV twist is usually unaffected early in the course of the disease. As the disease progresses and there is subepicardial involvement, LV twist decreases.[67] Net ventricular twist is negative in advanced DCM because of complete reversal of the LV apex rotation. Amyloid cardiomyopathy shows a relatively preserved magnitude of net LV twist angle, but the onset of untwisting is delayed after aortic valve closure in a healthy subject.

Diastolic indices can also be obtained by myocardial tagging, and may be useful in assessment of diastolic dysfunction in patients with HFpEF. Tissue tagging has helped identify heterogeneity in strain pattern in healthy individuals. Tagging of the right heart remains difficult due to the thin wall of the RV.[68]

The presence of pacemakers and ICDs has been considered a contraindication to MRI. In a study conducted by Nazarian and colleagues,[69] 555 MRI examinations were performed in 438 patients with devices (55% with permanent pacemaker and 45% with ICD) with monitoring and programming by a device nurse. There were no significant adverse events and only trivial changes seen in pacing parameters. The ability to perform MRI in patients with devices would expand the population of those with NICMP who can be studied using CMR.

Cardiac Computed Tomography

As CMR requires long acquisition times and excludes most patients with intracardiac devices, options for imaging with similar ability for tissue characterization are needed. Cardiac computed tomography (CCT) achieves excellent tissue characterization, with high spatial resolution in short acquisition times, and is now the gold standard for noninvasive angiography (Figure 9). When used in patients with cardiomyopathy, it can rule out ischemia as a cause, given its high negative predictive value.[70] With advances in technology in multidetector row CCT imaging, it is possible to accurately measure biventricular size and function, in addition to obtaining coronary imaging. Retrospective ECG gating allows for multiphase reformatting of the axial images in any plane covering the cardiac cycle from end-systole to end-diastole. Multiple studies comparing CCT with CMR have found good correlation between the two modalities for all measures of LV size and global function, including LV volume and LV mass.[71-74] In one study in which RV function was assessed, RVEF showed moderate agreement and RV volumes correlated

Multiple studies comparing CCT with CMR have found good correlation between the two modalities for all measures of LV size and global function, including LV volume and LV mass.

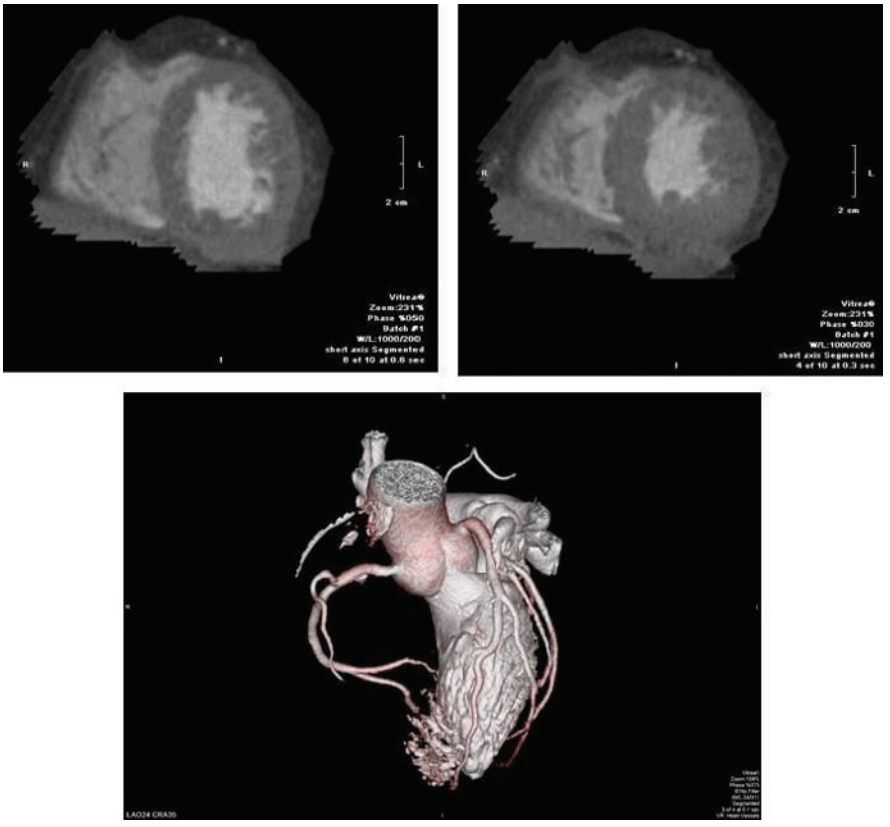

Figure 9. Cardiac computed tomography for evaluation of cardiomyopathy in a 57-year-old man with obesity prior to evaluation for an implantable cardioverter defibrillator. Images showed end-diastolic and end-systolic short-axis images of the left ventricle, and three-dimensional reconstruction of the coronary arteries. Gated images revealed normal biventricular size, concentric left ventricular hypertrophy, a left ventricular ejection fraction of 51%, and no valvular abnormalities. Coronary computed tomography angiography showed no coronary artery disease.

well between the two modalities,[62] though a major limitation was delineating RV contours due to inadequate contrast opacification.

With respect to specific causes of NICMP, asymmetric septal hypertrophy and systolic anterior motion of the mitral valve can be easily identified in patients with HCM.[75] In ARVD, RV dilatation with scalloping of the free wall, fat deposition in conspicuous trabeculae and the moderator band, and thinning of the RV wall have been described on CCT.[76] Moreover, extracardiac findings can aid in the diagnosis of systemic illnesses causing cardiomyopathy, such as hilar lymphadenopathy in sarcoidosis.

Quantitative analysis of LV strain using CCT was found to correlate well with echocardiography with regard to global and regional radial strain, CS, and LS, with fewer nondiagnostic LV segments and a shorter time for analysis.[77] This technique may be a valuable alternative for assessment of myocardial deformation in patients with poor echogenic windows and contraindications for MRI.

Newer Applications of Nuclear Scintigraphy

Nuclear scintigraphy is not a new imaging modality, but has recently found applicability in imaging cardiac amyloidosis, particularly ATTR amyloidosis, typically a difficult entity to diagnose. Radioisotopes used for skeletal imaging, such as ^{99m}Tc-3,3-diphospho-1,2-propanodicarboxylic acid (^{99m}Tc-DPD)[78] and ^{99m}Tc-pyrophosphate (^{99m}Tc-PYP),[79] have been found to concentrate in the hearts of patients with ATTR amyloidosis, but not as much in those with AL amyloidosis. ^{99m}Tc-PYP and ^{99m}Tc-DPD may bind TTR amyloid fibrils more intensely than AL fibrils as a result of higher calcium-containing compounds in ATTR hearts, and thus may be useful in distinguishing AL from ATTR cardiac amyloidosis, a distinction that impacts treatment. In a study of patients with ATTR cardiac amyloidosis who underwent ^{99m}Tc-diphosphonate imaging and CMR with LGE, although both modalities were similar in identifying myocardial amyloid deposition, the amyloid burden could be underestimated by visual analysis of CMR with LGE, thus suggesting that nuclear scintigraphy may actually be a superior technique for diagnosing ATTR amyloidosis.[80]

Imaging of Sympathetic Innervation of the Heart

Cardiac sympathetic nerves are preferentially stimulated in severe heart failure, with norepinephrine release from the failing heart at rest in untreated patients increased up to 50-fold, similar to the level of release in healthy hearts during near maximal exercise.[81] Myocardium of patients with chronic LV dysfunction shows significant reduction of presynaptic norepinephrine uptake and postsynaptic β-adrenoceptor density. Assessment of the degree of sympathetic activation of the heart can, therefore, be an indicator of the severity of the disease process. Efforts directed toward assessing sympathetic innervation of the heart led to development of radiotracers for single-photon emission computed tomography (SPECT) and positron emission tomography (PET) imaging. Imaging of sympathetic innervation is centered on the synaptic junction of the neuron,

and available radiotracers image presynaptic anatomy and function. Figure 10 shows adrenergic neurotransmitter synthesis, receptors, and norepinephrine transport in the cardiac presynaptic nerve terminal, along with radiopharmaceuticals available for the study of sympathetic innervation. The commonly used radiotracers are ^{123}I- metaiodobenzylguanidine (^{123}I-mIBG) for planar and SPECT imaging,[82] and ^{11}C-hydroxyephedrine for PET imaging.[83]

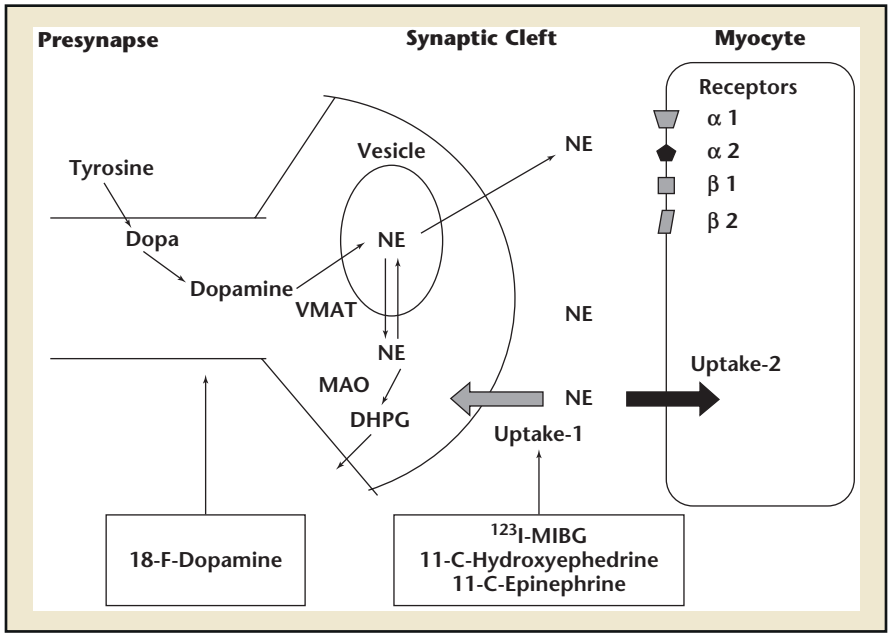

Figure 10. Diagram of adrenergic neurotransmitter synthesis, receptors, and norepinephrine transport in the cardiac presynaptic nerve terminal, along with radiopharmaceuticals available for the study of sympathetic innervation. DHPG, dihydroxyphenylglycol; MIBG, metaiodobenzylguanidine; MAO, monoamine oxidase; NE, norepinephrine; VMAT, vesicular monoamine transporter.

Imaging protocol with SPECT involves images obtained 15 to 30 minutes (early) and 3 to 4 hours (delayed) after intravenous injection of ^{123}I-mIBG. Myocardial uptake and distribution is visually assessed. The uptake of mIBG is semiquantified by calculating a heart-to-mediastinum ratio (H/M) after drawing regions of interest over the heart and mediastinum. The mIBG wash-out rate (WR) from the myocardium can be derived as ([early H/M-late H/M]/early H/M) × 100 (Figure 11). Reduced mIBG uptake in heart failure leads to reduced late H/M and increased WR (a measure of retention of norepinephrine by sympathetic neurons).[84]

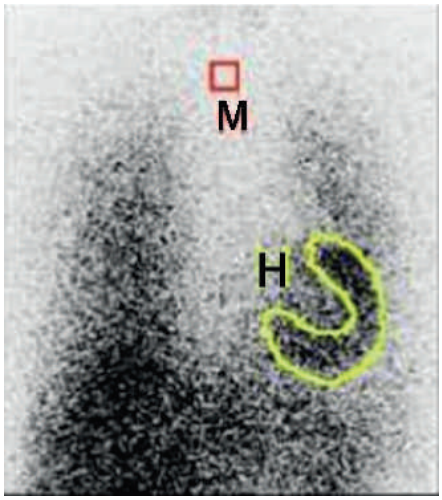

$$\text{H/M ratio} = \frac{\text{Heart region of interest mean count (H)}}{\text{Mediastinum mean count (M)}}$$

$$\text{Myocardial washout rate (WR)} = \frac{\{\text{H/M (immediate)- H/M (delayed)}\} \times 100}{\text{H/M (immediate)}}$$

H/M (immediate)- at 15 minutes

H/M (delayed)- at 4 hours

Figure 11. Quantification of cardiac ^{123}I- metaiodobenzylguanidine activity. Regions of interest are drawn over the heart and mediastinum in an anterior view of the thorax from which the heart-to-mediastinum (H/M) ratio and myocardial washout rate (WR) can be calculated.

A meta-analysis of 18 studies including 1755 patients indicated that heart failure patients with reduced late H/M or increased ^{123}I-mIBG WR have a worse prognosis compared with those with normal ^{123}I-mIBG uptake and WR parameters.[85] Subsequently the AdreView Myocardial Imaging for Risk Evaluation in Heart Failure (ADMIRE-HF) study,[86] which included 961 patients with NYHA class II/III heart failure and LVEF ≤ 35% who underwent imaging with ^{123}I-mIBG, revealed a lower cardiac event rate and higher 2-year survival rate in patients with H/M ≥ 1.6. These patients had a significantly lower rate of heart failure progression and arrhythmic events. The incidence of cardiac death in patients with H/M > 1.6 was < 1% per year, whereas it was 10-fold higher (9.6%) in those with H/M < 1.6.[86] Sympathetic innervation imaging also has a role in identifying patients with heart failure most likely to benefit from CRT. A prospective study of 45 heart failure patients undergoing CRT found higher baseline H/M

… commonly used radiotracers are ^{123}I- metaiodobenzylguanidine for planar and SPECT imaging, and ^{11}C-hydroxyephedrine for PET imaging.

ratio and lower WR with ^{123}I-mIBG imaging, with further improvement in these parameters following CRT in responders only.[87] A study of 50 patients undergoing CRT found the highest response rate (defined by decrease in LV end-systolic volume) in patients with evidence of LV dyssynchrony on echocardiography and H/M ratio ≥ 1.6.[88] In conclusion, available evidence points toward a role for sympathetic innervations imaging in patients with NICMP to predict risk of SCD prior to implantation of ICD and CRT devices. Sympathetic innervation in patients with LVAD using ^{123}I-mIBG has been evaluated in several small studies. In heart failure patients who had an LVAD implanted, there was a statistically significant improvement in early and delayed H/M ratio over 3 months of treatment with the LVAD,[89] suggesting that recovery of myocardial sympathetic innervation may be an important factor in functional recovery of the myocardium during LVAD support, and imaging with ^{123}I-mIBG might be used to evaluate the reverse remodeling occurring with long-term mechanical unloading of the heart.

… available evidence points toward a role for sympathetic innervations imaging in patients with NICMP to predict risk of SCD prior to implantation of ICD and CRT devices.

Positron Emission Tomography

PET utilizes radionuclide tracer techniques that produce images of in vivo radionuclides. PET allows noninvasive evaluation of myocardial blood flow, function, and metabolism, using physiologic substrates prepared with positron-emitting radionuclides (carbon, oxygen, nitrogen, and fluorine).[90] Alterations in myocardial substrate metabolism have been implicated in the pathogenesis of heart failure and contractile dysfunction.[91] In animal models of heart failure, the progression from cardiac hypertrophy to ventricular dysfunction is associated with downregulation of genes for fatty acid metabolism and a shift in metabolism to glucose as the primary fuel.[92] This has also been shown in patients with idiopathic DCM.[93]

In a study of 44 patients with advanced NICMP, matched perfusion and metabolism defects were seen on PET imaging in 91% of cases, with QRS duration on the surface ECG being positively correlated with the extent of the defect.[94] In a study using fluorodeoxyglucose (FDG) PET, worsening RV systolic function was associated with increased RV glucose uptake and increased ratio of uptake in the RV versus the LV.[95]

One of the more clinically relevant applications of PET imaging is in distinguishing cardiac sarcoidosis from other causes of NICMP using ^{18}F-labeled FDG (^{18}F-FDG). There is increased uptake in macrophage-dense regions, where the macrophages show a high metabolic rate, making them highly reliant on external glucose as a source of fuel.[96] In a meta-analysis of seven studies, pooled estimates for ^{18}F-FDG PET yielded 89% sensitivity and 78% specificity for diagnosis of cardiac sarcoid.[97] Increased uptake of FDG has been noted in cardiac sarcoid patients with ventricular tachycardia and advanced atrioventricular block.[98] In a study of 118 consecutive patients with known or suspected sarcoidosis who were referred for PET using ^{18}F-FDG to assess for inflammation and rubidium-82 to evaluate for perfusion defects, those with focal perfusion defects and cardiac FDG uptake had a higher risk of ventricular tachycardia and death.[99] In a longitudinal cohort of 23 patients with cardiac sarcoidosis, a reduction in the intensity and extent of myocardial inflammation on FDG PET was associated with improvement in LVEF, thus suggesting that serial PET scans could be used to monitor efficacy of immunosuppressive therapy in cardiac sarcoidosis.[100]

Conclusions

Newer imaging modalities can supplement traditional 2D echocardiographic examination and provide important information regarding etiology, cardiac mechanics, and prognosis in patients with NICMP. Additional imaging can help identify patients most likely to benefit from antiarrhythmic therapies such as ICD implantation and CRT, and risk stratify those for advanced heart failure therapies such as LVAD placement and cardiac transplantation. The role of fibrosis assessment and its implication for therapy is still being developed. Although some of these modalities (such as CMR) are increasingly being utilized, others, such as strain and sympathetic innervation imaging, are still not being used effectively. With increasing standardization of these moda-lities and their incorporation into guidelines, we are likely to see an increase in their use in the evaluation of patients with NICMP. ■

The authors report no real or apparent conflicts of interest or funding sources in the preparation of this manuscript.

References

1. Stecker EC, Vickers C, Waltz J, et al. Population-based analysis of sudden cardiac death with and without left ventricular systolic dysfunction: two-year findings from the Oregon Sudden Unexpected Death Study. *J Am Coll Cardiol*. 2006;47:1161-1166.
2. Pai RG, Jintapakorn W, Tanimoto M, et al. Three-dimensional echocardiographic reconstruction of the left ventricle by a transesophageal tomographic technique: in vitro and in vivo validation of its volume measurement. *Echocardiography*. 1996;13:613-622.
3. Hung J, Lang R, Flachskampf F, et al. 3D echocardiography: a review of the current status and future directions. *J Am Soc Echocardiogr*. 2007;20:213-233.
4. Siu SC, Rivera JM, Guerrero JL, et al. Three dimensional echocardiography: in vivo validation for left ventricular volume and function. *Circulation*. 1993;88:1715-1723.
5. Jacobs LD, Salgo IS, Goonewardena S, et al. Rapid quantification of left ventricular volumes from real-time three-dimensional echocardiographic data. *Eur Heart J*. 2006;27:460-468.
6. Fujimoto S, Mizuno R, Nakagawa Y, et al. Estimation of the right ventricular volume and ejection fractions by transthoracic three-dimensional echocardiography: validation study using magnetic resonance imaging. *Int J Card Imaging*. 1998;14:385-390.
7. Flachskampf FA, Chandra S, Gaddipatti A, et al. Analysis of shape and motion of the mitral annulus in subjects with and without cardiomyopathy by echocardiographic 3-dimensional reconstruction. *J Am Soc Echocardiogr*. 2000;13:277-287.
8. Kwan J, Shiota T, Agler DA, et al; Real-time three-dimensional echocardiography study. Geometric differences of the mitral apparatus between ischemic and dilated cardiomyopathy with significant mitral regurgitation: real-time three-dimensional echocardiography study. *Circulation*. 2003;107:1135-1140.
9. Marsan NA, Westenberg JJ, Ypenburg C, et al. Quantification of functional mitral regurgitation by real-time 3D echocardiography: comparison with 3D velocity-encoded cardiac magnetic resonance. *JACC Cardiovasc Imaging*. 2009;2:1245-1252.
10. Ton-Nu TT, Levine RA, Handschumacher MD, et al. Geometric determinants of functional tricuspid regurgitation: insights from 3-dimensional echocardiography. *Circulation*. 2006;114:143-149.
11. Kapetanakis S, Kearney MT, Siva A, et al. Real-time three-dimensional echocardiography: a novel technique to quantify global left ventricular mechanical dyssynchrony. *Circulation*. 2005;112:992-1000.
12. Mor-Avi V, Lang RM, Badano LP, et al. Current and evolving echocardiographic techniques for the quantitative evaluation of cardiac mechanics: ASE/EAE consensus statement on methodology and indications endorsed by the Japanese Society of Echocardiography. *J Am Soc Echocardiogr*. 2011;24:277-313.
13. Taber LA, Yang M, Podszus WW. Mechanics of ventricular torsion. *J Biomech*. 1996;29:745-752.
14. Geyer H, Caracciolo G, Abe H, et al. Assessment of myocardial mechanics using speckle tracking echocardiography: fundamentals and clinical applications. *J Am Soc Echocardiogr*. 2010;23:351-369.
15. Pirat B, Khoury DS, Hartley CJ, et al. A novel feature-tracking echocardiographic method for the quantitation of regional myocardial function: validation in an animal model of ischemia-reperfusion. *J Am Coll Cardiol*. 2008;51:651-659.
16. Chen J, Cao T, Duan Y, et al. Velocity vector imaging in assessing myocardial systolic function of hypertensive patients with left ventricular hypertrophy. *Can J Cardiol*. 2007;23:957-961.
17. Liu X, Li Z. Assessment of cardiac twist in dilated cardiomyopathy using velocity vector imaging. *Echocardiography*. 2010;27:400-405.
18. Brown J, Jenkins C, Marwick TH. Use of myocardial strain to assess global left ventricular function:

MAIN POINTS

- Echocardiography can quantify the severity of left ventricular (LV) systolic and diastolic dysfunction. However, in many instances, it does not identify the etiology of nonischemic cardiomyopathy (NICMP), as tissue characterization is not possible with routine echocardiography.
- Recent development of transesophageal and transthoracic multiplane ultrasound probes has enabled the acquisition of rotational images at defined interval angles around a fixed axis, leading to the development of three-dimensional (3D) echocardiography. Application of newer endocardial border detection techniques permits accurate assessment of LV volume, mass, and ejection fraction (EF) with 3D echocardiography, which is particularly useful in the appropriate selection of patients for implantable cardioverter defibrillator placement and cardiac resynchronization therapy.
- Tissue Doppler-derived strain and strain rate were the first methods used to quantify myocardial deformation, but angle dependence and noise interference make this method less desirable. Speckle-tracking echocardiography (STE) is an angle-independent method for strain analysis. Velocity-vector imaging (VVI) is an advanced echocardiographic method derived from STE. VVI is faster than conventional STE, and obtaining each patient's parameters takes approximately 5 minutes, which is faster than a routine STE study.
- Cardiac magnetic resonance (CMR) has emerged as a useful imaging modality for patients with cardiomyopathies. Cine CMR is used in the assessment of cardiac function and morphology by reconstructing electrocardiography-gated images. It provides accurate assessment of LV and right ventricular mass and volume, EF, and global and regional segmental wall motion. CMR is valuable in the identification of LV noncompaction cardiomyopathy, a rare form of NICMP. However, as CMR requires long acquisition times and excludes most patients with intracardiac devices, options for imaging with similar ability for tissue characterization are needed. Cardiac computed tomography achieves excellent tissue characterization, with high spatial resolution in short acquisition times, and is now the gold standard for noninvasive angiography.
- Assessment of the degree of sympathetic activation of the heart can be an indicator of the severity of the disease process. Efforts directed toward assessing sympathetic innervation of the heart led to development of radiotracers for single-photon emission computed tomography and positron emission tomography imaging. Imaging of sympathetic innervation is centered on the synaptic junction of the neuron, and available radiotracers image presynaptic anatomy and function.

a comparison with cardiac magnetic resonance and 3-dimensional echocardiography. *Am Heart J*. 2009;157:102.e1-102.e5.
19. Stanton T, Leano R, Marwick TH. Prediction of all-cause mortality from global longitudinal speckle strain: comparison with ejection fraction and wall motion scoring. *Circ Cardiovasc Imaging*. 2009;2: 356-364.
20. Zhang KW, French B, May Khan A, et al. Strain improves risk prediction beyond ejection fraction in chronic systolic heart failure. *J Am Heart Assoc*. 2014;3:e000550.
21. Kraigher-Krainer E, Shah AM, Gupta DK, et al; PARAMOUNT Investigators. Impaired systolic function by strain imaging in heart failure with preserved ejection fraction. *J Am Coll Cardiol*. 2014;63:447-456.
22. Carasso S, Yang H, Woo A, et al. Systolic myocardial mechanics in hypertrophic cardiomyopathy: novel concepts and implications for clinical status. *J Am Soc Echocardiogr*. 2008;21:675-683.
23. Paraskevaidis IA, Panou F, Papadopoulos C, et al. Evaluation of left atrial longitudinal function in patients with hypertrophic cardiomyopathy: a tissue Doppler imaging and two-dimensional strain study. *Heart*. 2009;95:483-489.
24. Phelan D, Collier P, Thavendiranathan P, et al. Relative apical sparing of longitudinal strain using two-dimensional speckle-tracking echocardiography is both sensitive and specific for the diagnosis of cardiac amyloidosis. *Heart*. 2012;98:1442-1448.
25. Buss SJ, Emami M, Mereles D, et al. Longitudinal left ventricular function for prediction of survival in systemic light-chain amyloidosis: incremental value compared with clinical and biochemical markers. *J Am Coll Cardiol*. 2012;60:1067-1076.
26. Miyoshi T, Tanaka H, Kaneko A, et al. Left ventricular endocardial dysfunction in patients with preserved ejection fraction after receiving anthracycline. *Echocardiography*. 2014;31:848-857.
27. Thavendiranathan P, Poulin F, Lim KD, et al. Use of myocardial strain imaging by echocardiography for the early detection of cardiotoxicity in patients during and after cancer chemotherapy: a systematic review. *J Am Coll Cardiol*. 2014;63:2751-2768.
28. Mercuro G, Cadeddu C, Piras A, et al. Early epirubicin-induced myocardial dysfunction revealed by serial tissue doppler echocardiography: correlation with inflammatory and oxidative stress markers. *Oncologist*. 2007;12:1124-1133.
29. Yu HK, Yu W, Cheuk DK, et al. New three-dimensional speckle-tracking echocardiography identifies global impairment of left ventricular mechanics with a high sensitivity in childhood cancer survivors. *J Am Soc Echocardiogr*. 2013;26:846-882.
30. Negishi K, Negishi T, Hare JL, et al. Independent and incremental value of deformation indices for prediction of trastuzumab-induced cardiotoxicity. *J Am Soc Echocardiogr*. 2013;26:493-498.
31. Hare JL, Brown JK, Leano R, et al. Use of myocardial deformation imaging to detect preclinical myocardial dysfunction before conventional measures in patients undergoing breast cancer treatment with trastuzumab. *Am Heart J*. 2009;158:294-301.
32. Plana JC, Galderisi M, Barac A, et al. Expert consensus for multimodality imaging evaluation of adult patients during and after cancer therapy: a report from the American Society of Echocardiography and the European Association of Cardiovascular Imaging. *J Am Soc Echocardiogr*. 2014;27:911-939.
33. Motoki H, Borowski AG, Shrestha K, et al. Right ventricular global longitudinal strain provides prognostic value incremental to left ventricular ejection fraction in patients with heart failure. *J Am Soc Echocardiogr*. 2014;27:726-732.
34. Cameli M, Bernazzali S, Lisi M, et al. Right ventricular longitudinal strain and right ventricular stroke work index in patients with severe heart failure: left ventricular assist device suitability for transplant candidates. *Transplant Proc*. 2012;44:2013-2015.
35. Grant AM, Smedira NG, Starling RC, Marwick TH. Independent and incremental role of quantitative right ventricular evaluation for the prediction of right ventricular failure after left ventricular assist device implantation. *J Am Coll Cardiol*. 2012;60:521-528.
36. Penicka M, Bartunek J, De Bruyne B, et al. Improvement of left ventricular function after cardiac resynchronization therapy is predicted by tissue Doppler imaging echocardiography. *Circulation*. 2004;109: 978-983.
37. Dohi K, Suffoletto MS, Schwartzman D, et al. Utility of echocardiographic radial strain imaging to quantify left ventricular dyssynchrony and predict acute response to cardiac resynchronization therapy. *Am J Cardiol*. 2005;96:112-116.
38. Marwick TH, Leano RL, Brown J, et al. Myocardial strain measurement with 2-dimensional speckle-tracking echocardiography: definition of normal range. *JACC Cardiovasc Imaging*. 2009;2:80-84.
39. Cannesson M, Tanabe M, Suffoletto MS, et al. Velocity vector imaging to quantify ventricular dyssynchrony and predict response to cardiac resynchronization therapy. *Am J Cardiol*. 2006;98:949-953.
40. Chung ES, Leon AR, Tavazzi L, et al. Results of the Predictors of Response to CRT (PROSPECT) trial. *Circulation*. 2008;117:2608-2616.
41. Bax JJ, Gorcsan J, III. Echocardiography and noninvasive imaging in cardiac resynchronization therapy: results of the PROSPECT (Predictors of Response to Cardiac Resynchronization Therapy) study in perspective. *J Am Coll Cardiol*. 2009;53:1933-1943.
42. Weiford BC, Subbarao VD, Mulhern KM. Noncompaction of the ventricular myocardium. *Circulation*. 2004;109:2965-2971.
43. Petersen SE, Selvanayagam JB, Wiesmann F, et al. Left ventricular non-compaction: insights from cardiovascular magnetic resonance imaging. *J Am Coll Cardiol*. 2005;46:101-105.
44. Gulati A, Jabbour A, Ismail TF, et al. Association of fibrosis with mortality and sudden cardiac death in patients with nonischemic dilated cardiomyopathy. *JAMA*. 2013;309:896-908.
45. Leyva F, Taylor RJ, Foley PW, et al. Left ventricular midwall fibrosis as a predictor of mortality and morbidity after cardiac resynchronization therapy in patients with nonischemic cardiomyopathy. *J Am Coll Cardiol*. 2012;60:1659-1667.
46. Kuruvilla S, Adenaw N, Katwal AB, et al. Late gadolinium enhancement on cardiac magnetic resonance predicts adverse cardiovascular outcomes in nonischemic cardiomyopathy: a systematic review and meta-analysis. *Circ Cardiovasc Imaging*. 2014;7:250-258.
47. Masci PG, Doulaptsis C, Bertella E, et al. The incremental prognostic value of myocardial fibrosis in patients with non-ischemic cardiomyopathy without congestive heart failure. *Circ Heart Fail*. 2014;7:448-456.
48. Takashio S, Yamamuro M, Uemura T, et al. Correlation between extent of myocardial fibrosis assessed by cardiac magnetic resonance and cardiac troponin t release in patients with nonischemic heart failure. *Am J Cardiol*. 2014;113:1697-1704.
49. Cain MA, Metzl MD, Patel AR, et al. Cardiac sarcoidosis detected by late gadolinium enhancement and prevalence of atrial arrhythmias. *Am J Cardiol*. 2014;113:1556-1560.
50. Moon JC, Messroghli DR, Kellman P, et al; Society for Cardiovascular Magnetic Resonance Imaging; Cardiovascular Magnetic Resonance Working Group of the European Society of Cardiology. Myocardial T1 mapping and extracellular volume quantification: a Society for Cardiovascular Magnetic Resonance (SCMR) and CMR Working Group of the European Society of Cardiology consensus statement. *J Cardiovasc Magn Reson*. 2013;15:92.
51. Kellman P, Hansen MS. T1-mapping in the heart: accuracy and precision. *J Cardiovasc Magn Reson*. 2014;16:2.
52. Iles L, Pfluger H, Phrommintikul A, et al. Evaluation of diffuse myocardial fibrosis in heart failure with cardiac magnetic resonance contrast-enhanced T1 mapping. *J Am Coll Cardiol*. 2008;52:1574-1580.
53. Flett AS, Hayward MP, Ashworth MT, et al. Equilibrium contrast cardiovascular magnetic resonance for the measurement of diffuse myocardial fibrosis: preliminary validation in humans. *Circulation*. 2010;122:138-144.
54. Tadamura E, Yamamuro M, Kubo S, et al. Effectiveness of delayed enhanced MRI for identification of cardiac sarcoidosis: comparison with radionuclide imaging. *AJR Am J Roentgenol*. 2005;185:110-115.
55. Patel MR, Cawley PJ, Heitner JF, et al. Detection of myocardial damage in patients with sarcoidosis. *Circulation*. 2009;120:1969-1977.
56. Ise T, Hasegawa T, Morita Y, et al. Extensive late gadolinium enhancement on cardiovascular magnetic resonance predicts adverse outcomes and lack of improvement in LV function after steroid therapy in cardiac sarcoidosis. *Heart*. 2014;100:1165-1172.
57. Greulich S, Deluigi CC, Gloekler S, et al. CMR imaging predicts death and other adverse events in suspected cardiac sarcoidosis. *JACC Cardiovasc Imaging*. 2013;6:501-511.
58. Maceira AM, Joshi J, Prasad SK, et al. Cardiovascular magnetic resonance in cardiac amyloidosis. *Circulation*. 2005;111:186-193.
59. Dungu JN, Valencia O, Pinney JH, et al. CMR-based differentiation of AL and ATTR cardiac amyloidosis. *JACC Cardiovasc Imaging*. 2014;7:133-142.
60. Deux JF, Damy T, Rahmouni A, et al. Noninvasive detection of cardiac involvement in patients with hereditary transthyretin associated amyloidosis using cardiac magnetic resonance imaging: a prospective study. *Amyloid*. 2014;21:246-255.
61. Castillo E, Lima JA, Bluemke DA. Regional myocardial function: advances in MR imaging and analysis. *Radiographics*. 2003;23(Spec No):S127-S140.
62. Jung B, Markl M, Föll D, Hennig J. Investigating myocardial motion by MRI using tissue phase mapping. *Eur J Cardiothorac Surg*. 2006;29(suppl 1):S150-S157.
63. Kanzaki H, Nakatani S, Yamada N, et al. Impaired systolic torsion in dilated cardiomyopathy: reversal of apical rotation at mid-systole characterized with magnetic resonance tagging method. *Basic Res Cardiol*. 2006;101:465-470.
64. Young AA, Kramer CM, Ferrari VA, et al. Three dimensional left ventricular deformation in hypertrophic cardiomyopathy. *Circulation*. 1994;90:854-867.
65. Carasso S, Yang H, Woo A, et al. Systolic myocardial mechanics in hypertrophic cardiomyopathy: novel concepts and implications for clinical status. *J Am Soc Echocardiogr*. 2008;21:675-683.
66. Carasso S, Woo A, Yang H, et al. Myocardial mechanics explains the time course of benefit for septal ethanol ablation for hypertrophic cardiomyopathy. *J Am Soc Echocardiogr*. 2008;21:493-499.
67. Sengupta PP, Tajik AJ, Chandrasekaran K, Khandheria BK. Twist mechanics of the left ventricle: principles and application. *JACC Cardiovasc Imaging*. 2008;1:366-376.
68. Jeung MY, Germain P, Croisille P, et al. Myocardial tagging with MR imaging: overview of normal and pathologic findings. *Radiographics*. 2012;32:1381-1398.
69. Nazarian S, Hansford R, Roguin A, et al. A prospective evaluation of a protocol for magnetic resonance imaging of patients with implanted cardiac devices. *Ann Intern Med*. 2011;155:415-424.
70. Budoff MJ, Dowe D, Jollis JG, et al. Diagnostic performance of 64-multidetector row coronary computed tomographic angiography for evaluation of coronary artery stenosis in individuals without known coronary artery disease: results from the prospective multicenter ACCURACY (Assessment by Coronary Computed Tomographic Angiography of Individuals Undergoing Invasive Coronary Angiography) trial. *J Am Coll Cardiol*. 2008;52:1724-1732.
71. Dewey M, Müller M, Eddicks S, et al. Evaluation of global and regional left ventricular function with 16-slice computed tomography, biplane cineventriculography, and two-dimensional transthoracic echocardiography: comparison with magnetic resonance imaging. *J Am Coll Cardiol*. 2006;48:2034-2044.
72. Wu YW, Tadamura E, Kanao S, et al. Left ventricular functional analysis using 64-slice multidetector row computed tomography: comparison with left

ventriculography and cardiovascular magnetic resonance. *Cardiology*. 2008;109:135-142.
73. Schlosser T, Mohrs OK, Magedanz A, et al. Assessment of left ventricular function and mass in patients undergoing computed tomography (CT) coronary angiography using 64-detector-row CT: comparison to magnetic resonance imaging. *Acta Radiol*. 2007;48: 30-35.
74. Raman SV, Shah M, McCarthy B, et al. Multi-detector row cardiac computed tomography accurately quantifies right and left ventricular size and function compared with cardiac magnetic resonance. *Am Heart J*. 2006;151:736-744.
75. Gopalan D, Raj V, Hoey ET. Cardiac CT: non-coronary applications. *Postgrad Med J*. 2010;86:165-173.
76. Kimura F, Sakai F, Sakomura Y, et al. Helical CT features of arrhythmogenic right ventricular cardiomyopathy. *Radiographics*. 2002;22:1111-1124.
77. Buss SJ, Schulz F, Mereles D, et al. Quantitative analysis of left ventricular strain using cardiac computed tomography. *Eur J Radiol*. 2014;83:e123-e130.
78. Rapezzi C, Quarta CC, Guidalotti PL, et al. Role of (99m)Tc-DPD scintigraphy in diagnosis and prognosis of hereditary transthyretin-related cardiac amyloidosis. *JACC Cardiovasc Imaging*. 2011;4:659-670.
79. Bokhari S, Castaño A, Pozniakoff T, et al. (99m)Tc-pyrophosphate scintigraphy for differentiating light-chain cardiac amyloidosis from the transthyretin-related familial and senile cardiac amyloidoses. *Circ Cardiovasc Imaging*. 2013;6:195-201.
80. Minutoli F, Di Bella G, Mazzeo A, et al. Comparison between (99m)Tc-diphosphonate imaging and MRI with late gadolinium enhancement in evaluating cardiac involvement in patients with transthyretin familial amyloid polyneuropathy. *AJR Am J Roentgenol*. 2013;200:W256-W265.
81. Eisenhofer G, Friberg P, Rundqvist B, et al. Cardiac sympathetic nerve function in congestive heart failure. *Circulation*. 1996;93:1667-1676.
82. Kline RC, Swanson DP, Wieland DM, et al. Myocardial imaging in man with I-123 meta-iodobenzylguanidine. *J Nucl Med*. 1981;22:129-132.
83. Thackeray JT, Bengel FM. Assessment of cardiac autonomic neuronal function using PET imaging. *J Nucl Cardiol*. 2013;20:150-165.
84. Agostini D, Carrio I, Verberne HJ. How to use myocardial 123I-MIBG scintigraphy in chronic heart failure. *Eur J Nucl Med Mol Imaging*. 2009;36:555-559.
85. Verberne HJ, Brewster LM, Somsen GA, van Eck-Smit BL. Prognostic value of myocardial 123I-metaiodobenzylguanidine (MIBG) parameters in patients with heart failure: a systematic review. *Eur Heart J*. 2008;29:1147-1159.
86. Jacobson AF, Senior R, Cerqueira MD, et al; ADMIRE-HF Investigators. Myocardial iodine-123 meta-iodobenzylguanidine imaging and cardiac events in heart failure. Results of the prospective ADMIRE-HF (AdreView Myocardial Imaging for Risk Evaluation in Heart Failure) study. *J Am Coll Cardiol*. 2010;55: 2212-2221.
87. Cha YM, Chareonthaitawee P, Dong YX, et al. Cardiac sympathetic reserve and response to cardiac resynchronization therapy. *Circ Heart Fail*. 2011;4:339-344.
88. Tanaka H, Tatsumi K, Fujiwara S, et al. Effect of left ventricular dyssynchrony on cardiac sympathetic activity in heart failure patients with wide QRS duration. *Circ J*. 2012;76:382-389.
89. Drakos SG, Athanasoulis T, Malliaras KG, et al. Myocardial sympathetic innervation and long-term left ventricular mechanical unloading. *JACC Cardiovasc Imaging*. 2010;3:64-70.
90. Gewirtz H. Cardiac PET: a versatile, quantitative measurement tool for heart failure management. *JACC Cardiovasc Imaging*. 2011;4:292-302.
91. Liao R, Nascimben L, Friedrich J, et al. Decreased energy reserve in an animal model of dilated cardiomyopathy: relationship to contractile performance. *Circ Res*. 1996;78:893-902.
92. Barger PM, Kelly DP. Fatty acid utilization in the hypertrophied and failing heart: molecular regulatory mechanisms. *Am J Med Sci*. 1999;318:36-42.
93. Dávila-Román VG, Vedala G, Herrero, et al. Altered myocardial fatty acid and glucose metabolism in idiopathic dilated cardiomyopathy. *J Am Coll Cardiol*. 2002;40:271-277.
94. O'Neill JO, McCarthy PM, Brunken RC, et al. PET abnormalities in patients with nonischemic cardiomyopathy. *J Card Fail*. 2004;10:244-249.
95. Mielniczuk LM, Birnie D, Ziadi MC, et al. Relation between right ventricular function and increased right ventricular [18F]fluorodeoxyglucose accumulation in patients with heart failure. *Circ Cardiovasc Imaging*. 2011;4:59-66.
96. Ohira H, Tsujino I, Ishimaru S, et al. Myocardial imaging with 18F-fluoro-2-deoxyglucose positron emission tomography and magnetic resonance imaging in sarcoidosis. *Eur J Nucl Med Mol Imaging*. 2008;35:933-941.
97. Youssef G, Leung E, Mylonas I, et al. The use of 18F-FDG PET in the diagnosis of cardiac sarcoidosis: a systematic review and metaanalysis including the Ontario experience. *J Nucl Med*. 2012;53:241-248.
98. McArdle BA, Birnie DH, Klein R, et al. Is there an association between clinical presentation and the location and extent of myocardial involvement of cardiac sarcoidosis as assessed by ^{18}F-fluorodoexyglucose positron emission tomography? *Circ Cardiovasc Imaging*. 2013;6:617-626.
99. Blankstein R, Osborne M, Naya M, et al. Cardiac positron emission tomography enhances prognostic assessments of patients with suspected cardiac sarcoidosis. *J Am Coll Cardiol*. 2014;63:329-336.
100. Osborne MT, Hulten EA, Singh A, et al. Reduction in ^{18}F-fluorodeoxyglucose uptake on serial cardiac positron emission tomography is associated with improved left ventricular ejection fraction in patients with cardiac sarcoidosis. *J Nucl Cardiol*. 2014;21: 166-174.